Indian Journal of Chemistry
Vol. 61, February 2022, pp. 127-135

Unveiling the reactions of triethylphosphite and its diethylamino substituted derivatives to carbon tetrachloride with a molecular electron density theory perspective

Ali Barhoumi[a], Mohammed Salah[a], Abdellah Zeroual[a], Mrinmoy Chakraborty[b] & Nivedita Acharjee[c,]*

[a]Molecular Modeling and Spectroscopy Research Team, Department of Chemistry, Faculty of Sciences, Chouaïb Doukkali University, El Jadida, Morocco

[b]Department of Electronics and Communication Engineering, Dr. B. C. Roy Engineering College, Durgapur-713 206, West Bengal, India

[c]Department of Chemistry, Durgapur Government College, Durgapur-713 214, West Bengal, India

*E-mail: nivchem@gmail.com

Received 29 August 2021; revised and accepted 04 January 2022

A molecular electron density theory study is presented herein for the reactions of triethylphosphite (TEP) and its diethylamino substituted derivatives (DEAP and MEAP) to carbon tetrachloride (CCl_4). Analysis of the Electron localization function (ELF) has allowed characterizing the electronic structure of the reagents and the conceptual density functional theory (CDFT) study predicted the polar character of the reactions with the electronic flux from TEP, DEAP and MEAP to CCl_4. Analysis of the relative energies along the potential energy surfaces has indicated energetically favoured attack on the chlorine atom of CCl_4 relative to that on the carbon atom and the reactions became energetically more facile due to introduction of the electron donating diethylamino substituent. This allowed formulating the heterolytic mechanism of the reactions in which the quick exchange of CCl_3^- with the chlorine atom takes place for TEP, while the exchange is slowed down in DEAP and MEAP due to mesomeric stabilization of the phosphonium ion. The ELF and Atoms in molecules (AIM) studies indicated early transition states (TSs) with no new covalent bond formation, and the non-covalent interactions at the interatomic bonding regions of the TSs are analysed from the Independent Gradient Model (IGM) analysis based on the Hirshfield partition of electron density.

Keywords: Triethylphosphite, Electron Localization Function, MEDT, Transition state, NCI

Organophosphorus compounds (OPs) exhibit a broad spectrum of potential applications in medicine[1-3], as pesticides[4], as flame retardants and plasticizers[5] and as chemical warfare agents[6]. Very recently, Satnami *et al*. have reported the N-Doped Carbon Quantum Dot-MnO_2 Nanowire FRET Pairs for detection[7] and the glutathione (GSH)-capped CdTe quantum dot (QD)-based fluorescence assay for the monitoring of organophosphate pesticides[8]. Demkowicz *et al.*[1] reviewed the biological activities of the OPs while Costa[9] has explained their toxicological effects in 2018. The OPs contain organic moeities either directly bonded to phosphorus or through a heteroatom. The reactivity of OPs have been focussed since the last five decades, and the reaction of triethylphosphite TEP **1** with carbon tetrachloride CCl_4 **2** leading to diethyl trichloromethyl phosphonate is among the most studied ones from the mechanistic point of view. This reaction was first formulated as a homolytic one following a radical chain mechanism (Scheme 1), supporting acceleration of the reaction in presence of UV light or dibenzoyl peroxide[10].

Walling and coworkers[11] proposed an alternate mechanism (Scheme 2) involving the ethyl radical which was discounted since no disproportionation or dimerization products of the ethyl radical were obtained. Cadogan and Foster[12] studied the reactions of substituted phosphites with carbon tetrachloride and formulated two mechanisms, the radical one was supported by the observed acceleration in UV light and dibenzoyl peroxide, while the possibility of heterolytic mechanism was implied from the reaction taking place in dark or in absence of radical initiators. This mechanistic duality was further investigated by Cadogan and Sharp in 1966[13], and in 1969, Atkinson *et al.*[14] concluded the heterolytic mechanism (Scheme 3) for the thermal reaction of triethylphosphite TEP **1** with CCl_4 **2**.

Finally, in 1987, a comprehensive study by Bakkas and coworkers[10] confirmed the ionic heterolytic

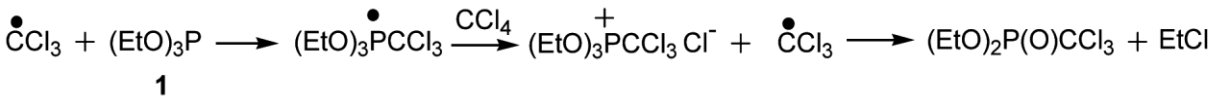

Scheme 1 — Radical Chain mechanism for the reaction of TEP **1** with CCl_4 **2**

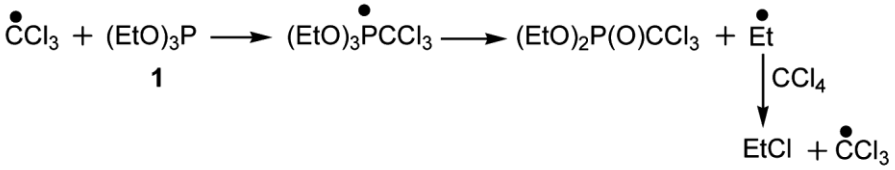

Scheme 2 — Radical Chain mechanism involving ethyl radical for the reaction of TEP **1** with CCl_4 **2**

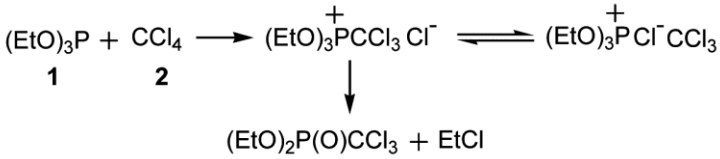

Scheme 3 — Heterolytic mechanism for the thermal reaction of TEP **1** with CCl_4 **2**

mechanism as the primary one under thermal conditions in agreement with Cadogan *et al.*[12,13], while the participation of the radical pathway increases in presence of UV light and radical initiators.

The molecular electron density theory (MEDT) framework proposed by Domingo in 2016[15] identifies the decisive role of the changes in electron density in the molecular reactivity. MEDT uses a set of quantum chemical tools to characterise the changes in electron density and has been successfully applied in the last five years[16,17] to analyze several chemical reactions in terms of chemoselectivity[18,19], regioselectivity[20,21], stereoselectivity[22,23], catalysis[24,25], strain promotion[26,27], and substituent effects[28]. Herein, we have applied the quantum chemical tools within the MEDT framework to analyze the reactions of TEP [$P(OEt)_3$] **1** and its diethylamino substituted derivatives DEAP [$P(NEt_2)(OEt)_2$] **3** and MEP [$P(NEt_3)(OEt)$] **4** with CCl_4 **2** at B3LYP/6-311G(d,p) level of theory. The study has been divided into four sections. (i) A topological analysis of the Electron localization function[29,30](ELF) of the reagents **1** - **4** was performed to know the electronic structures (ii) The conceptual density functional theory[31,32] (CDFT) analysis is performed to comprehend the direction of electronic flux and the polar character (iii) The stationary points along the potential energy surface (PES) of the feasible approach modes are located and the energy profile is analyzed along with the Global Electron Density Transfer[33] (GEDT) calculations at the TSs (iv) The topological analysis of the ELF[29,30] and the Atoms in Molecules (AIM) proposed by Bader and coworkers[34,35] is performed at the located transition states (TSs) along with the characterization of the non-covalent interactions (NCI[36]) in terms of the newly proposed Independent Gradient Model[37] (IGM) based on the Hirshfield partition of electron density[38] (IGMH).

Experimental Details

Computational Methods

The stationary points along the PES for the reactions of TEP **1**, DEAP **3**, MEP **4** with CCl_4 **2** were optimized using the B3LYP[39,40] functional with the conjunction of 6-311G(d,p) basis set allowing a satisfactory quality/cost ratio for the size of the investigated systems. The Berny analytical gradient optimization method[41] was applied for the optimizations. The local minima (No. of imaginary frequency = 0) and the TSs (No. of imaginary frequency = 1) were verified from the frequency calculations and the intrinsic reaction coordinate (IRC) calculations allowed verifying the minimum energy reaction path using the González-Schlegel integration method[42,43].

The conceptual density functional theory (CDFT) reactivity indices namely the electronic chemical potential μ and chemical hardness η, were calculated using the following equations[44,31,32]

$$\mu \approx (E_{HOMO} + E_{LUMO})/2 \quad \ldots (1)$$

$$\eta \approx E_{LUMO} - E_{HOMO} \quad \ldots (2)$$

where HOMO (E_{HOMO}) and LUMO (E_{LUMO}) energies are calculated at B3LYP/6-31G(d) computational level to characterise the reagents within the standard electrophilicity[45] and nucleophilicity[46] scales.

The electrophilicity index ω is expressed in terms of μ and η as:

$$\omega = \mu^2/2\eta \quad \ldots (3)$$

The relative nucleophilicity index[46] N is expressed as

$$N = E_{HOMO} - E_{HOMO(tetracyanoethylene)} \quad \ldots (4)$$

where, $E_{HOMO(tetracyanoethylene)}$ is the HOMO energy of tetracyanoethylene used as the reference for the nucleophilicity scale[46].

The global electron density transfer[33] (GEDT) at the located TSs was calculated using the formula,

$$GEDT\ (f) = \sum_{q \in f} q, \quad \ldots (5)$$

where GEDT is computed as the sum of the natural atomic charges (q) derived from the natural population analysis[47,48] (NPA) of the atoms belonging to each reacting framework(f) at the TSs. Positive GEDT indicates electronic flux from the corresponding reacting counterpart. All calculations were performed using the Gaussian 09 suite of programs[49].

The topological analysis of the ELF[29,30] and the AIM[34,35] were performed using Multiwfn software[50]. The ELF localization domains were visualized using UCSF Chimera software[51]. The IGMH studies were performed using the Multiwfn software and the respective isosurfaces were visualized using the VMD software[52].

Results and Discussion

ELF Topological analysis of the reagents

The ELF constructed by Becke and Edgecombe[29] and further illustrated by Silvi and Savin[30] allows establishing the electronic structure by characterizing the core, bonding and non-bonding regions of chemical structures. The ELF localization domains of the reagents **1**-**4** are represented in Fig. 1 while the total integrating population of the most significant ELF valence basins are given in Table S1 of the Supplementary Data. The proposed Lewis like structures on the basis of ELF valence basin populations are represented in Scheme 4. The ELF of TEP **1** shows monosynaptic basins V(O1), V(O2) & V'(O2), V(O3) & V'(O3) integrating a total population of 4.77, 4.85 and 4.88 e, respectively, associated with the non bonding electron density of O1, O2 and O3 oxygen. The disynaptic basins V(P,O1), V(P,O2) and V(P,O3) show the total integrating population of 1.57, 1.46 and 1.41 e, respectively, associated with the underpopulated P-O1, P-O2 and P-O3 single bonds. The ELF of DEAP **3** shows monosynaptic basins V(O2) & V'(O2) and V(O3) & V'(O3) integrating a total population of 4.85 and 4.90 e, respectively, associated with the non bonding electron density of O2 and O3 oxygen, while the monosynaptic V(N1) basin integrating 1.69 e is associated with the non bonding electron density at N1 nitrogen. The disynaptic basins V(P,N1), V(P,O2) and V(P,O3) show the total integrating population of 2.63, 1.45 and 1.39 e, respectively, associated with the P-N1, P-O2 and P-O3 single bonds. The ELF of MEAP **4** shows monosynaptic basins V(O3) & V'(O3) integrating a total population of 4.88 e associated with the non bonding electron density of O3 oxygen, while the monosynaptic V(N1) and V(N2) & V'(N2) basins integrate a total population of 1.74 e and 2.64 e associated with the non bonding electron density at N1 and N2 nitrogen. The disynaptic basins V(P,N1), V(P,N2) and V(P,O3) show the total integrating population of 2.62, 1.70 and 1.38 e, respectively, associated with the P-N1, P-N2 and P-O3 single bonds. The ELF of TEP **1**, DEAP **3** and MEAP **4** also

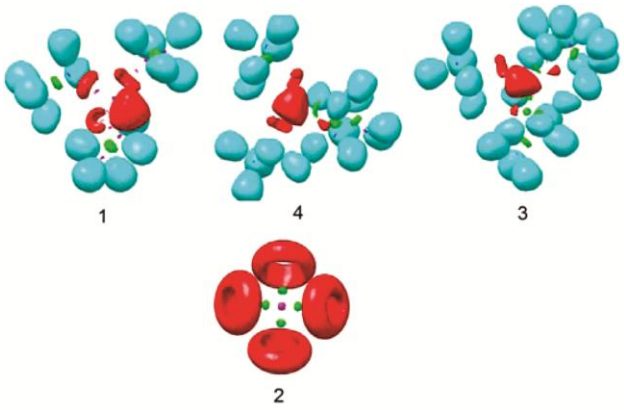

Fig. 1 — B3LYP/6-311G(d,p) ELF localization domains of optimized TEP **1**, DEAP **3**, MEAP **4** and CCl_4 **2** The protonated basins are shown in blue, disynaptic basins are shown in green, monosynaptic basins are shown in red and core basins are shown in magenta colour

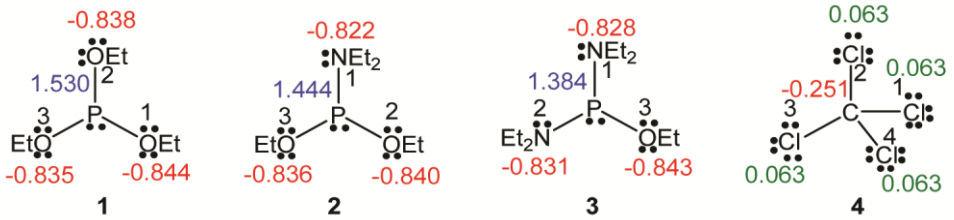

Scheme 4 — The natural atomic charges at the reacting centres of the proposed Lewis-like structures of TEP **1**, DEAP **3**, MEAP **4** and CCl_4 **2** are given in average number of electrons e. Red, green and blue colours represent negative, negligible and positive NBO charges, respectively

show the presence of monosynaptic basin V(P) integrating 2.23, 2.23 and 2.19 e, respectively. The ELF of CCl_4 shows the presence of monosynaptic basins each integrating a total population of 6.39 e associated with the non bonding electron density at Cl1, Cl2, Cl3 and Cl4. The disynaptic basins V(C,Cl1), V(C,Cl2), V(C,Cl3) and V(C,Cl4) intergrate the total population of 1.55, 1.51, 1.53 and 1,48 e associated with the respective C-Cl single bonds.

For TEP **1**, DEAP **3** and MEAP **4**, oxygen and nitrogen atoms are negatively charged by -0.822 to -0.844 e, while the phosphorus atom is positively charged by 1.530 e, 1.444 e and 1.384 e, respectively, for TEP **1**, DEAP **3** and MEAP **4**, indicating the substituent effects.

Analysis of the global and local reactivity indices of the reagents

Analysis of the global reactivity indices defined within the CDFT[30,31] allows comprehending the direction of electronic flux and the polar character of chemical reactions. The CDFT indices of reagents **1** - **4** are given in Table 1. The electronic chemical potential μ of **1** (μ = -2.70 eV), **3** (μ = -2.37 eV) and **4** (μ = -2.08 eV) show higher values than that of CCl_4 **2** (μ = -5.48 eV), suggesting the electronic flux from the the reagents **1**, **3** and **4** to CCl_4. TEP **1**, DEAP **3**, MEAP **4** are classified as the marginal electrophiles (ω < 0.80 eV) within the electrophilicity scale[45], while CCl_4 **2** as the strong electrophile (ω > 1.50 eV) with the electrophilicity ω = 2.23 eV, indicating polar reactions. Within the nucleophilicity scale[46], CCl_4 is classified as the weak nucleophile (N = 0.29 eV), **1** (N = 2.65 eV) as the moderate nucleophile while both **3** (N = 3.11 eV) and **4** (N = 3.77 eV) as the strong nucleophiles. Thus, along the investigated reactions, CCl_4 **2** will act as the electrophile, and the reagents TEP **1**, DEAP **3** and MEAP **4** as the nucleophiles.

Table 1 — B3LYP/6-31G(d) calculated CDFT indices namely, the electronic chemical potential μ, global hardness η, electrophilicity ω and nucleophilicity indices N (in eV) of the reagents **1-4**

	μ	η	ω	N
1	-2.70	7.54	0.48	2.65
3	-2.37	7.28	0.39	3.11
4	-2.08	6.55	0.33	3.77
2	-5.48	6.71	2.23	0.29

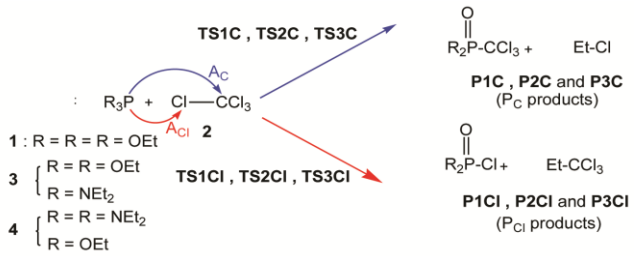

Scheme 5 — Reactions of CCl_4 **2** with TEP **1**, DEAP **3**, MEAP **4**

Analysis of the potential energy surfaces associated with the reactions of TEP 1, DEAP 3, MEAP 4 with CCl_4 2

For the reactions of TEP **1**, DEAP **3** and MEAP **4** with CCl_4 **2**, there are two feasible regioisomeric approach modes, namely the nucleophilic attack of phosphorus on the carbon atom or the chlorine atom of CCl_4 **2** (Scheme 5). Search for the stationary points along these two feasible approaches allowed locating the reactants **1** - **4**, products **P1C**, **P2C**, **P3C,** respectively, for the attack on the carbon atom and the corresponding TSs **TS1C**, **TS2C**, **TS3C**, while products **P1Cl**, **P2Cl**, **P3Cl**, respectively, were located for the attack on the chlorine atom and the corresponding TSs **TS1Cl**, **TS2Cl**, **TS3Cl** (Scheme 5). The relative energies, enthalpies, entropies and free energies of the TSs and the products are given in Table 2, while the total energies, enthalpies, entropies and free energies are listed in Table S2 of the Supplementary Material. The energy profile is represented in Fig. 2.

The energy profile study allowed arriving at some appealing conclusions (1) The reactions of CCl_4 **2**

Table 2 — B3LYP/6-311G(d,p) calculated relative energies (kcal mol^{-1}), enthalpies (kcal mol^{-1}), entropies (cal mol^{-1} K^{-1}) and free energies (kcal mol^{-1}) of the TSs and the products associated with the reactions of **1, 3** and **4** with **2**

	ΔE	ΔH	ΔS	ΔG	GEDT
TS1C	54.3	55.1	-30.9	64.3	0.99
P1C	-23.7	-23.0	0.9	-23.3	
TS1Cl	38.7	39.3	-19.7	45.2	0.70
P1Cl	-45.3	-44.2	1.3	-44.6	
TS2C	53.1	54.1	-38.7	65.6	0.96
P2C	-26.5	-25.5	-2.4	-24.8	
TS2Cl	34.2	34.9	-27.7	43.1	0.73
P2Cl	-50.3	-48.9	-2.1	-48.3	
TS3C	47.6	49.4	-31.5	58.8	0.94
P3C	-24.4	-22.7	1.8	-23.2	
TS3Cl	27.3	28.7	-20.5	34.8	0.64
P3Cl	-52.1	-50.0	5.1	-51.5	

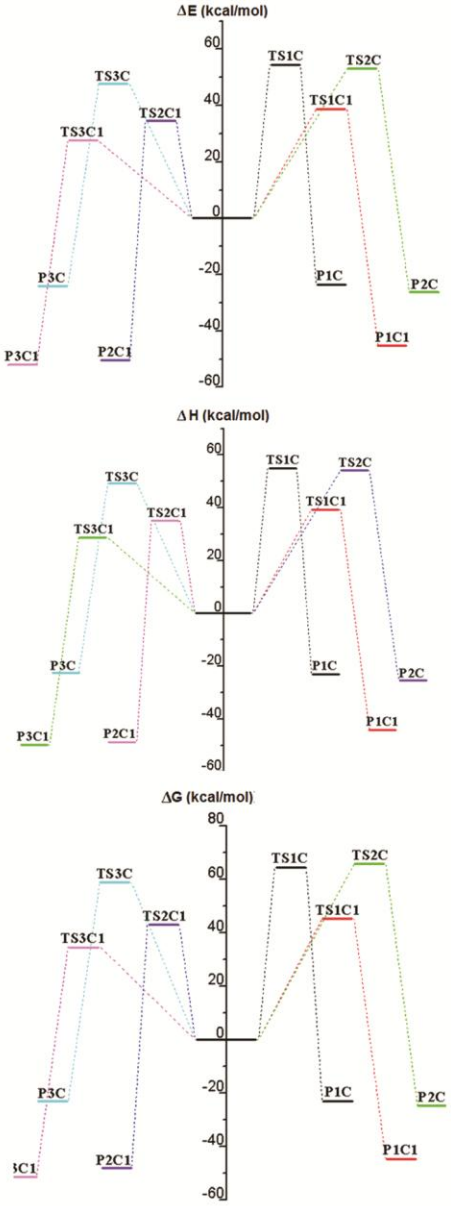

Fig. 2 — Energy profile of the studied reactions

with TEP **1**, DEAP **3**, MEAP **4** along the carbon and the chlorine approach modes show negative Gibbs free energies between -23.2 kcal mol^{-1} (**P3C**) to -51.5 kcal mol^{-1} (**P3Cl**) and hence are irreversible and under kinetic control. (2) For the reaction of TEP **1** with CCl_4 **2**, the activation energy of **TS1Cl** is lowered than that of **TS1C** by 15.6 kcal mol^{-1}**.** Following the similar trend, the activation energies of **TS2Cl** and **TS3Cl** are lowered than that of **TS2C** and **TS3C** by 18.9 kcal mol^{-1} and 20.3 kcal mol^{-1}, respectively. This predicts energetic preference for the attack on the chlorine atom. (3) Note that the free energy of activation of **TS1Cl** is lowered than that of **TS1C** by 19.1 kcal mol^{-1}, and that of **TS2Cl** and **TS3Cl** are lowered than that of **TS2C** and **TS3C** by 22.5 kcal mol^{-1} and 24 kcal mol^{-1}, respectively, suggesting that the nucleophilic attack of phosphorus on the the chlorine atom of CCl_4 **2** is energetically more feasible in MEAP **4** relative to DEAP **3** and TEP **1** in complete agreement with the experimental results (Table 3) (4) The reaction (attack of the phosphorus atom on the chlorine atom) of MEAP **4** is energetically favoured by 6.9 kcal mol^{-1} compared to that of DEAP **3**, while activation energy of the reaction of DEAP **3** is lowered than that of TEP **1** by 4.5 kcal mol^{-1}. The experimental results[10,14] (Table 3) suggest different proportions of the P_C and P_{Cl} products (Scheme 5) depending on the nature of the substituents. (5) The activation free energies are increased by 5.9-11.5 kcal mol^{-1} relative to the enthalpy of activation, while the free energies of reaction are comparable to the enthalpies of reaction due to minimal reaction entropies in each case.

The geometry of the TSs associated with the reactions of the TEP **1**, DEAP **3**, MEAP **4** with CCl_4 **2** are given in Fig. 3. It is evident that the P-C and P-Cl are greater than 2.28 Å in each case suggesting that

Table 3 — Proportions of the P_C and P_{Cl} products (Scheme 5) products obtained from the reactions of TEP **1**, DEAP **3**, MEAP **4,** and $(Et_2N)_3P$ **5** with CCl_4 **2**

R_3P	% P_C	% P_{Cl}
$P(OEt)_3$ (TEP **1**)	100	Traces
$(Et_2N)P(OEt)_2$ (DEAP **3**)	75-80	20-25
$(Et_2N)_2P(OEt)$ (MEAP **4**)	25-30	70-75
$(Et_2N)_3P$ **5**	--------	--------

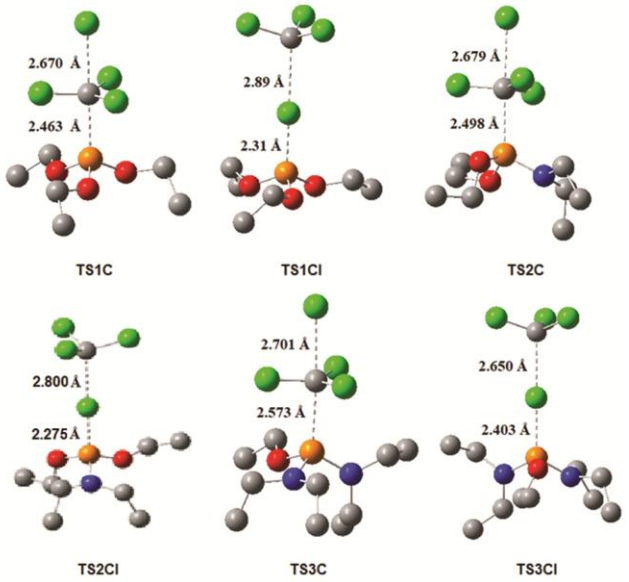

Fig. 3 —Geometry of the TSs associated with the reactions of TEP **1**, DEAP **3**, MEAP **4** and CCl_4 **2**

the formation of new covalent bonds has not taken place at the TSs. This is in complete agreement with the topological analysis of the ELF and the QTAIM.

Finally, the global electron density transfer (GEDT) at the TSs was calculated to assess the polar character and are listed in Table 2. All six TSs showed GEDT[33] values greater than 0.20 e, suggesting highly polar reactions with electronic flux from TEP **1**, DEAP **3**, MEAP **4** towards the CCl_4 **2** in complete agreement with the CDFT analysis as discussed before.

Now, considering the experimental results (Table 3) and the relative energies of the TSs (Table 2), the heterolytic ionic mechanism (proposed by Cadogan *et al.*[12-14] and confirmed by Bakkas *et al.*[10]) of the investigated reactions is represented in Scheme 6. The first step involves the energetically feasible nucleophilic attack of TEP **1**, DEAP **3**, MEAP **4** on the chlorine atom of CCl_4 **2** resulting in the ion pair $R_1R_2P^+(OEt)Cl, CCl_3^-$ (P1). The carbanion CCl_3^- being highly reactive is quickly exchanged with chlorine to give the P2 ion pair leading to the

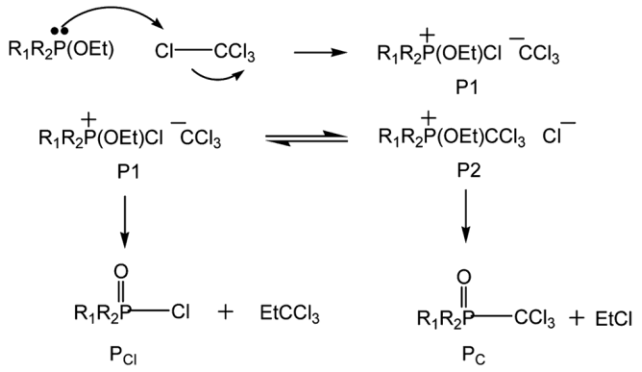

Scheme 6 — Mechanism of the reactions of TEP **1**, DEAP **3**, MEAP **4** with CCl_4 **2**

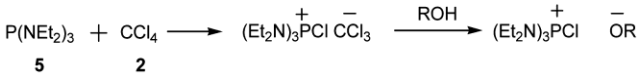

Scheme 7 — Reaction of $(Et_2N)_3P$ **5** with CCl_4 **2**

P_C product. This exchange reaction slows down when the phosphorus atom carries electron donor groups, such as the substituent diethylamino(Et_2N-). The latter stabilizes the phosphonium ion by mesomeric effect, which would allow the P1 ion pair to evolve towards the P_{Cl} type product.

Note that the lowering of the activation energy (Table 2) is observed for reactions of TEP **1**, DEAP **3** and MEAP **4**, following the reactivity order: $(Et_2N)_2P(OEt) > (Et_2N)P(OEt)_2 > P(OEt)_3$.

It was also observed that for $(Et_2N)_3P$ **5**, the reaction did not progress to the products P_C and P_{Cl} since an alkoxy $(RO-)$ group is required for the reaction. In the presence of alcohol, chloroform is formed. This indicates the formation of the carbanion $\overline{C}Cl_3$ following an attack of type A_{Cl} (Scheme 7)

Topological Analysis of the ELF and the AIM at the TSs associated with the reactions of the trivalent phosphorus derivatives 1- 3 with CCl_4 4

The concept of ELF was constructed by Becke and Edgecombe[29] to define a precise mathematical representation of the Lewis valence theory for molecular systems. Silvi and Savin[30] further extended the ELF to define three basic types of localization attractors, namely the core, bonding and non-bonding attractors, and the basins represent the topological partititoning of the ELF gradient fields. Valence basins are associated with the bonding and non-bonding regions, while the core basins surround the atomic nuclei. The presence of monosynaptic basins V(A) is associated with the lone pairs or

pseudoradical centers. The disynaptic basin V(A,B) is associated with the bonding regions between two atoms A and B.. The integration of electron density over the volume of the basins allows obtaining a quantitative analysis and this mathematical representation allows comprehending a straightforward connection of the electronic structure and molecular reactivity. The ELF localization domain of the **TS1C**, **TS1Cl**, **TS2C**, **TS2Cl**, **TS3C** and **TS3Cl** are shown in Fig. 4 and the most significant ELF valence basin populations of **TS1C** and **TS1Cl** are listed in Table S3 of the Supplementary data. The ELF of **TS1C** and **TS1Cl** show the presence of monosynaptic basins associated with the non bonding electron densities at the three chlorine atoms of CCl_4 **4** and the monosynaptic V(C) integrating 1.53 e and 1.73 e

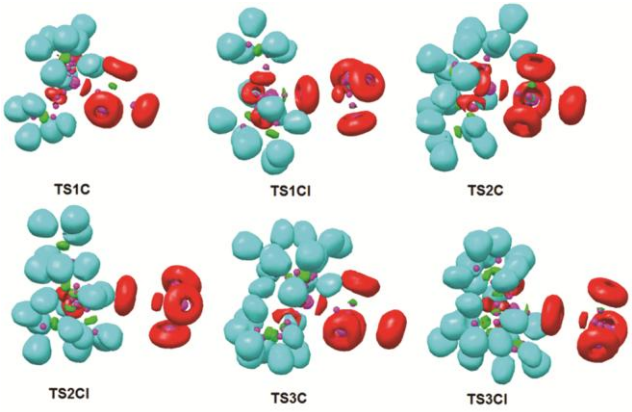

Fig. 4 — B3LYP/6-311G(d,p) calculated most significant ELF localization domains at the TSs associated with the reactions of TEP 1, DEAP 3, MEAP 4 and CCl_4 2. The attractor positions are shown as magenta coloured spheres. The protonated basins are shown in blue, disynaptic basins are shown in green, monosynaptic basins are shown in red

respectively at **TS1C** and **TS1Cl** is also observed which is absent in CCl_4 (Fig. 1) and is associated with the formation of carbenoid[53] centre (monosynaptic basin integrating greater than 1 e) at the CCl_4 carbon along the reaction path. Note that the monosynaptic V(P) basin undergoes depopulation from 2.23 e to 1.90 e in **TS1C** and 1.51 in **TS1Cl**. The ELF of both TSs do not show the presence of disynaptic basins associated with the formation of new P-C or P-Cl bonds, which is in conformity with the forming bond lengths at the TSs and the topological analysis of the AIM.

Finally, an AIM topological analysis[34,35] of the electron density ρ at **TS1C**, **TS1Cl**, **TS2C**, **TS2Cl**, **TS3C** and **TS3Cl** was performed at the bond critical points (BCPs) corresponding to the interatomic bonding regions. The total electron density ρ and the Laplacian of electron density $\nabla^2\rho(r_c)$ at the BCPs are given in Table 4 while the bond paths and the BCPs are shown in Fig. 5. **CP1-CP6** correspond to the BCPs located between the chlorine atoms of CCl_4 and hydrogen atoms of TEP **1**, DEAP **2**, MEAP **3**. **CP1-CP6** show very low electron densities and positive Laplacian of electron density suggesting non-covalent interactions. **CP7** is associated with the BCP of the C-Cl bond of CCl_4 which is cleaved during the reaction. The low electron density at **CP7** is observed in each case with positive Laplacian of electron density suggesting non-covalent interactions. **CP8** is associated with the BCP of the forming P-C bond in **TS1C, TS2C** and **TS3C** and the forming P-Cl bond in **TS1Cl, TS2Cl** and **TS3Cl**. Note that the total electron densities at **CP8** of **TS1Cl, TS2Cl** and **TS3Cl** are 0.089, 0.095 and 0.075 while that at **TS1C, TS2C** and **TS3C** are 0.061, 0.057 and 0.005, respectively

Table 4 — Total electron density, ρ (a.u.) and Laplacian of electron density $\nabla^2\rho(r_c)$ (a.u.) at the BCPs **CP1-CP8** of the TSs associated with the reactions of TEP **1**, DEAP **3**, MEAP **4** and CCl_4 **2**

	CP1(H-Cl)		CP2 (H-Cl)		CP3 (H-Cl)		CP4 (H-Cl)		CP5 (H-Cl)		CP6 (H-Cl)		CP7 (C-Cl)		CP8 (P-C/Cl)	
	ρ	$\nabla^2\rho(r_c)$	ρ	$\nabla^2\rho(r_c)$	ρ	$\nabla^2\rho(r_c)$	ρ	$\nabla^2\rho(r_c)$	ρ	$\nabla^2\rho(r_c)$	ρ	$\nabla^2\rho(r_c)$	ρ	$\nabla^2\rho(r_c)$	ρ	$\nabla^2\rho(r_c)$
TS1C	0.004	0.013	0.006	0.018	0.004	0.013							0.033	0.048	0.061	0.022
TS1Cl													0.025	0.04	0.089	0.056
TS2C	0.006	0.019	0.004	0.013	0.007	0.023							0.033	0.048	0.057	0.025
TS2Cl	0.005	0.016											0.028	0.048	0.095	0.035
TS3C	0.005	0.017	0.006	0.019	0.006	0.02	0.008	0.025	0.031	0.047	0.05	0.027	0.007	0.025	0.005	0.018
TS3Cl	0.009	0.032											0.037	0.056	0.075	0.069

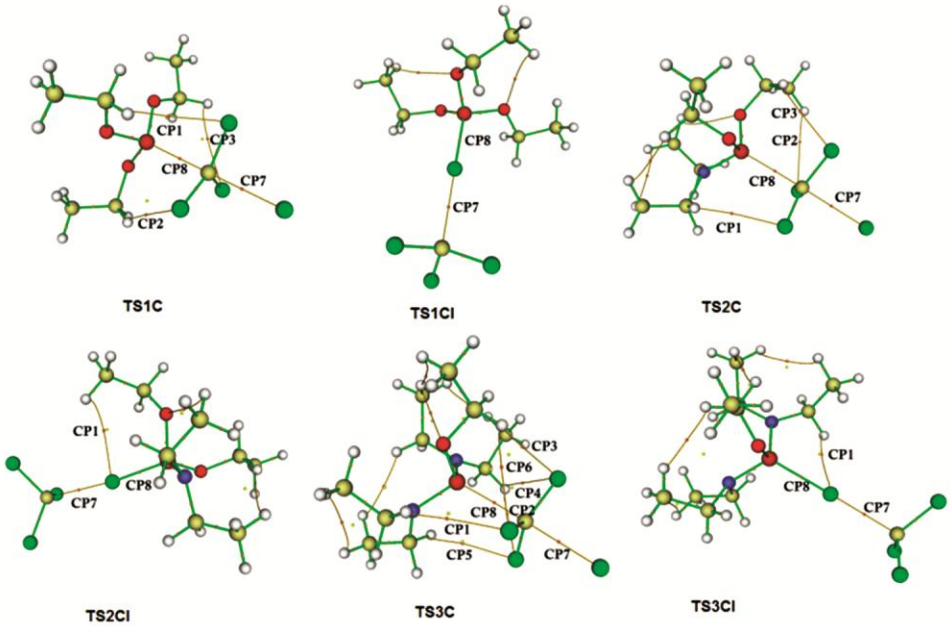

Fig. 5 — BCPs CP1-CP8 (shown as orange dots) and the bond paths (shown in yellow colour) at the TSs associated with the reactions of TEP **1**, DEAP **3**, MEAP **4** and CCl_4 **2**

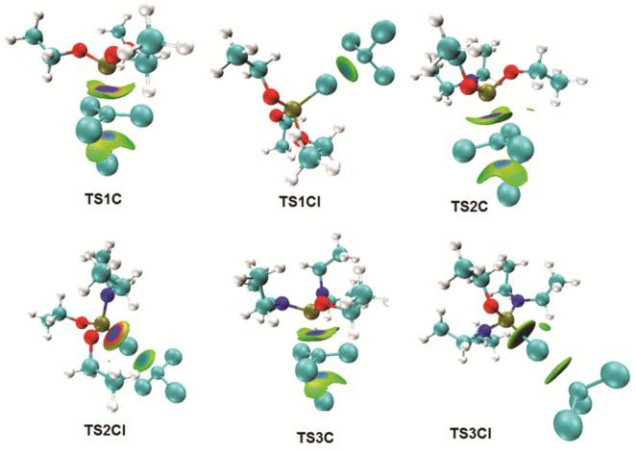

Fig. 6 — IGMH isosurfaces (Isovalue= 0.01) at the TSs associated with the reactions of TEP **1**, DEAP **3**, MEAP **4** and CCl_4 **2**

suggesting greater accumulation of electron densities along the TSs associated with approach mode to chlorine atom. The positive Laplacian suggests no new covalent bond formation at the TSs in complete agreement with the ELF study.

The recently proposed IGM[37] based on the Hirshfield partition of electron density[38] allows characterizing the non-covalent interactions[36] (NCI) at the TSs. The IGMH isosurfaces of **TS1C**, **TS2C**, **TS3C**, **TS1Cl**, **TS2Cl** and **TS3Cl** are given in Fig. 6. Note that strong attractive (blue portions) non-covalent interactions are observed in each of the TSs at the P-C and P-Cl forming bond regions and repulsive non-covalent interactions (red portions) are also observed in some of the TSs. The IGMH isosurfaces also show weak (green portions) and small traces of strong attractive (blue portions) non-covalent interactions at the C-Cl bonding region which is cleaved along the reaction path.

Conclusion

The reactions of triethylphosphite TEP **1**, and its substituted diethylamino derivatives DEAP **3** and MEAP **4** with carbon tetrachloride **2** have been studied within the molecular electron density theory (MEDT) framework. The topological analysis of the ELF and the NBO derived charges allowed characterizing the electronic structure and the bonding as well as the non bonding electron densities at the reacting centres. The CDFT analysis predicts polar character of the reactions. The electronic chemical potentials suggest electronic flux from TEP **1**, DEAP **3** and MEAP **4** to CCl_4 **2**. The reagents **1**, **3** and **4** are classified as the marginal electrophiles and CCl_4 **2** as the strong electrophile within the electrophilicity scale. The energy profile study suggests lowered activation energies along the approach mode of TEP **1**, DEAP **3**, MEAP **4** on the chlorine atom of CCl_4 **2** relative to that along the carbon atom of CCl_4 **2** by 15.6, 18.9 and 20.3 kcal mol^{-1}. The activation energy is decreased due to introduction of electron donating diethylamino substituent in the triethylphosphite,

allowing formulation of the ionic heterolytic mechanism involving the quick exchange of the carbanion CCl_3^- with the chlorine atom which slows down in DEAP **3** and MEAP **4** due to mesomeric stabilization of the phosphonium ion. The topological analysis of the ELF and the AIM suggested no new covalent bond formation at the located TSs and the non-covalent interactions at the BCPs could be characterized from the IGMH analysis at the interatomic bonding regions of the TSs.

Supplementary Data

Supplementary data associated with this article are available in the electronic form at http://nopr.niscair.res.in/jinfo/ijca/IJCA_61(02)YYYY-YYYY_SupplData.pdf.

References

1 Demkowicz S, Rachon J, Dasko M & Kozak W, *RSC Adv*, 6 (2016) 7101.
2 Akbaş H, Okumuş A, Kılıç Z, Hökelek T, Süzen Y, Koç L Y, Açık L & Çelik Z B, *Eur J Med Chem*, 70 (2013) 294.
3 Dabrzalska M, Zablocka M, Mignani S, Majoral J P & Klajnert-Maculewicz B, *Int J Pharm*, 492 (2015) 266.
4 Pope C N, *J Toxicol Environ Health B Crit Rev*, 2 (1999) 161.
5 Andresen J A, Grundmann A & Bester K, *Sci Total Environ*, 332 (2004) 155.
6 Delfino R T, Ribeiro T S & Figueroa-Villa J D, *J Braz Chem Soc*, 20 (2009) 407.
7 Dewangan L, Korram J, Karbhal I, Nagwanshi R & Satnami M L, *ACS Appl Nano Mater* 4 (2021) 13612.
8 Korram J, Dewangan L, Karbhal I, Nagwanshi R, Vaishanav S K, Ghosh K K & Satnami M L, *RSC Adv*, 10 (2020) 24190.
9 Costa L G, *Toxicol Sci*, 162 (2018) 24.
10 Bakkas S, Julliard M & Chanon M, *Tetrahedron*, 43 (1987) 501.
11 Walling C & Rabinowitz R, *J Am Chem Soc*, 81 (1959) 1243.
12 Cadogan J I G & Foster W R, *J Chem Soc*, (1961) 3071.
13 Cadogan J I G & Sharp J T, *Tetrahedron Lett*, 7 (1966) 2733.
14 Atkinson R E, Cadogan J I G & Sharp J T, *J Chem Soc B*, (1969)138.
15 Domingo L R, *Molecules*, 21 (2016) 1319.
16 Rioz-Gutiérrez M & Domingo L R, *Eur J Org Chem*, (2019) 267.
17 Domingo L R & Acharjee N, *Frontiers in Computational Chemistry*, (Bentham and Science, Singapore) 2000, p 174.
18 Domingo L R , Rioz-Gutiérrez M & Acharjee N, *Molecules*, 24 (2019) 832.
19 Domingo L R & Acharjee N, *ChemistrySelect*, 6 (2021) 4521.
20 Domingo L R , Rioz-Gutiérrez M & Pérez P, *J Org Chem*, 83 (2018) 2182.
21 Acharjee N, Salim H M, Chakraborty M, Rao M P & Ganesh M, *J Phys Org Chem*, 34 (2021) e4189 .
22 Acharjee N & Banerji A, *J Chem Sci*, 132 (2020) 65.
23 Acharjee N, *Struct Chem*, 31 (2020) 2147.
24 Domingo L R, Rioz-Gutiérrez M & Pérez P, *J Org Chem*, 83 (2018) 10959.
25 Domingo L R & Acharjee N, *J Phys Org* Chem, 33 (2020) e4062.
26 Domingo L R & Acharjee N, *New J Chem* 44 (2020)13633.
27 Domingo L R & Acharjee N, *J Phys Org Chem*, 33 (2020) e4100.
28 Domingo L R & Acharjee N, *ChemistrySelect*, 3 (2018) 8373.
29 Becke A D & Edgecombe K E, *J Chem Phys*, 92 (1990) 5397.
30 Silvi B & Savin A, *Nature*, 371 (1994) 683.
31 Geerlings P, De Proft F & Langenaeker W, *Chem Rev*, 103 (2003) 1793.
32 Domingo L R , Ríos-Gutiérrez M & Pérez P, *Molecules*, 21 (2016) 748.
33 Domingo L R, *RSC Adv*, 4 (2014) 32415.
34 Bader R F W, *Atoms in Molecules: A Quantum Theory* (Oxford Clarendon Press, USA) 1990.
35 Bader R F W & Essén H, *J Chem Phys*, 80 (1984) 1943.
36 García J C-, Johnson E R, Keinan S, Chaudret R, Piquemal J -P, Beratan D N & Yang W, *J Chem Theory Comput*, 73 (2011) 625.
37 Lefebvre C, Khartabil H, Boisson J -C, García J C-, Piquemal J- P & Hénon E, *ChemPhysChem*, 19 (2018) 724.
38 De Proft F, V-Reyes R, Peeters A, Alsenoy C Von & Geerlings P, *J Comput Chem*, 24 (2003) 463.
39 Becke A D, *Phys Rev A*, 38 (1988) 3098.
40 Lee C, Yang W & Parr R G, *Phys Rev B*, 37 (1988) 785.
41 Schlegel H B, *J Comput Chem*, 3 (1982) 214.
42 González C & Schlegel H B, *J Phys Chem*, 94 (1990) 5523.
43 González C & Schlegel H B, *J Chem Phys*, 95 (1991) 5853.
44 Parr R G & Yang W, *Density functional theory of atoms and molecules* (Oxford University Press, New York) 1989
45 Domingo L R, Aurell M J, Perez P & Contreras R, *Tetrahedron*, 58 (2002) 4417.
46 Domingo L R & Pérez P, *Org Biomol Chem*, 9 (2011) 7168.
47 Reed A E, Weinstock R B & Weinhold F, *J Chem Phys*, 83 (1985) 735.
48 Reed A E, Curtiss L A & Weinhold F, *Chem Rev*, 88 (1988) 899.
49 Frisch M J et al Gaussian 09, Gaussian Inc, Wallingford CT, (2009)
50 Lu T & Chen F, *J Comp Chem*, 33 (2012) 580.
51 Pettersen E F, Goddard T D, Huang C C, Couch G S, Greenblatt D M, Meng E C & Ferrin T E, *J Comput Chem*, 25 (2004) 1605.
52 Humphrey W, Dalke A & Schulten K, *J Mol Graph*, *14* (2005) 33.
53 Ríos-Gutiérrez M & Domingo L R, *Tetrahedron*, 75 (2019) 1961.